Journal of Environmental Chemical Engineering 9 (2021) 105343

Contents lists available at ScienceDirect

Journal of Environmental Chemical Engineering

journal homepage: www.elsevier.com/locate/jece

Dual-function ZIF-8 membrane supported on alumina hollow fiber membrane for copper(II) removal

Dayang Norafizan binti Awang Chee [a,b], Farhana Aziz [a,*], Ahmad Fauzi Ismail [a,*], Mohamed Afizal bin Mohamed Amin [a,c], Mohd. Sohaimi Abdullah [a]

[a] Advanced Membrane Technology Research Centre (AMTEC), School of Chemical and Energy Engineering, Faculty of Engineering, Universiti Teknologi Malaysia, 81310, Johor Bahru, Johor Darul Takzim, Malaysia
[b] Faculty of Resource Science and Technology, Universiti Malaysia Sarawak, 94300 Kota Samarahan, Sarawak, Malaysia
[c] Department of Chemical Engineering and Energy Sustainability, Faculty of Engineering, Universiti Malaysia Sarawak, 94300 Kota Samarahan, Sarawak, Malaysia

ARTICLE INFO

Editor: Dr. GL Dotto

Keywords:
ZIF-8 membranes
Alumina
Natural-based materials
Copper(II) removal
Adsorptive membranes

ABSTRACT

The as-spun alumina hollow fiber membrane was used as membrane support for the development of ZIF-8 membrane. The ZIF-8 layers were successfully grown on the support by using the in-situ solvothermal method and layer-by-layer method. The morphology and physicochemical properties of the membranes were characterized using the field emission scanning electron microscope (FESEM), X-ray diffraction spectrophotometer (XRD), Fourier-Transform Infrared Spectrophotometer (FTIR). The adsorption study revealed that the removal of copper(II) ion was pH-dependent. The adsorption capacity for copper(II) adsorption is 76.5 mg/g. The adsorption mechanism of copper(II) onto the ZIF-8 membrane was best fitted to the Freundlich isotherm and pseudo-second-order model. The filtration study showed that the membranes could remove up to 90% of copper(II) ions from the aqueous solution.

1. Introduction

Water is the source of life. Each person on Earth needs at least 20–50 L of clean water for daily activities, including drinking, cooking and cleaning. Consuming polluted water is a major concern and need to be taken care of because it might cause death to human and life-beings. The industrialization has grown at a very fast rate, contributed to the demand for natural resources. The mining activities have led to environmental pollution due to the release of inorganic ions, organic pollutants, organometallic compounds, radioactive isotopes and nanoparticles [1].

Heavy metal wastewater originated from urbanization and industrialization activities, leading to heavy metal accumulation in the water bodies. The high solubility of heavy metals in aquatic environments leads to the high potential to be absorbed by living organisms. Thus, the accumulation of heavy metal throughout the food chain will cause harmful effects, especially to humans, as the concentration will increase along the food chain. The common heavy metals present in industrial wastewater include nickel, zinc, silver, lead, iron, chromium, copper, arsenic, cadmium and uranium [2]. However, copper was found to be in higher concentrations among all the heavy metals because it is commonly used in industrial applications. The United State Environmental Protection Agency (USEPA) has determined that drinking water should have less than 1.3 ppm of copper [2].

Several methods and techniques were reported previously on the removal of copper ions from wastewater, for example, the adsorption [3–5], photocatalysis [6], electrochemical [7], chemical precipitation [8,9], ion exchange [10] and flotation [11,12]. Although a vast number of techniques were employed for copper(II) removal, new technologies with better performance and advantages still being searched to overcome some advantages from the previous method, for instance, the incomplete removal, high energy requirements and the production of toxic waste after the treatment [13]. Therefore, membrane technologies come into the picture to facilitate the removal of pollutants and water recovery.

In the present study, alumina hollow fiber membrane, derived from natural-based material known as alumina, was selected as a support membrane. Alumina is a naturally occurred aluminium oxide, found in the environment as minerals known as corundum, diaspore and gibbsite [14]. Alumina originated from bauxite, the impure form of gibbsite. The bauxite undergoes extraction process to purify the compounds into a

* Corresponding authors.
E-mail addresses: farhana@petroleum.utm.my (F. Aziz), afauzi@utm.my (A.F. Ismail).

https://doi.org/10.1016/j.jece.2021.105343
Received 21 January 2021; Received in revised form 25 February 2021; Accepted 8 March 2021
Available online 12 March 2021

usable form. One of the most used processes is the Bayer process [15]. Alumina is the most useful oxide ceramic due to its hard property and ability to withstand harsh environment, for example, high acidity or high basicity condition and its resistance towards high temperature. These attributes making it suitable to be used in various applications includes membrane separation applications.

Alumina has known to offer better water separations than the polymer-type membranes, not only because of the properties mentioned previously but also due to its resistance towards fouling. Alumina stable upon the defouling process, which usually require heat and the application of chemicals, thus the use of alumina can reduce the operation cost for separation process [14]. Inevitably, there are challenges to reduce the pore size of the natural-based support layer due to its coarse particle size and also the pores inside the particles [16]. The porous structure produced from the properties mentioned makes the rejection of copper(II) almost impossible. To further improve the support membrane's surface pore size, a layer of ZIF-8 membranes was deposited on top of the alumina hollow fiber membrane, producing an adsorptive membrane. The adsorptive membrane synergizes the advantages and functions of adsorbent and membrane at the same time. ZIF-8, a type of metal-organic framework with an aperture size of 0.34 nm, composed of zinc atoms and 2-methylimidazolate as ligands [17]. The adjustable cage is making it suitable for various applications. The ZIF-8 have shown excellent performance in the various field includes water treatment [18–20], gas separation [21,22] and medical applications [23]. Therefore, ZIF-8 was selected in this study to develop the dual-function membrane, commonly known as the adsorptive membrane. The embedding of ZIF-8 layer on top of the alumina support layer is believed to improve the performance of the membrane. Adsorptive membranes are known to have the affinity for ions and molecules and may combine ions by chelating effects, complexation and ion exchange [24]. Few studies were reported on the hybrid membrane for copper(II) removal [25,26]. However, there are still no reports on the application of ZIF-8 membrane on alumina hollow fiber membrane support to remove copper(II) ions. Therefore, the present study was conducted to prepare, characterize, and determine the prepared membranes' adsorption and filtration performance for copper(II) ions removal.

2. Experimental

2.1. Materials

2.1.1. Alumina hollow fiber preparation

Al_2O_3 powder with the size of 1 μm (99.9%), 0.5 μm (99.5%), 0.01 μm (99.8%) purchased from Alfa Aesar, Arlacel P135 (Uniqema), polyethersulfone (PESf, Radal A300, Ameco Performance), and N-methyl-2-pyrrolidone (NMP) (AR grade, Qrec) as the solvent.

2.1.2. APTES modification

3-(aminopropyl)triethoxysilane (APTES) (99%)(Sigma-Aldrich), Toluene (ACS reagent, Merck).

2.1.3. ZIF-8 Membrane Preparation

zinc nitrate hexahydrate ($Zn(NO_3)_2.6H_2O$,98%, Sigma-Aldrich), 2-methylimidazole (99%, Acros Organics), sodium formate (ACS Reagent, Acros Organics) and dimethylformamide (ACS reagent, Merck).

2.2. Preparation of alumina hollow fiber support

The alumina hollow fiber membrane support was prepared via the phase-inversion and sintering technique. The details of the fabrication process can be found elsewhere [27]. Alumina powder with different particle size (0.01 μm:0.05 μm:1 μm) at a ratio of 5:3:2 was used to prepare the membrane suspension. The suspension composed of 53 wt% of alumina, 36.87 wt% of N-methyl-2-pyrrolidone (NMP) and 1.3 wt% of Arlacel, was rotated and milled in a planetary ball mill (model: NQM-2 Planetary ball mill) for 48 h before the addition of polyethersulfone as polymer binder (8.83 wt%) the process was continued for another 48 h before the degassing process was executed for gas or bubble removal. The spinning process was performed by flowing the mixtures into a tube-in orifice (OD = 3 mm, ID = 2.8 mm) at 9 mL min^{-1} through a syringe pump (Harvard Equipment). Water was flowed at 10 mL min^{-1} through the center of the spinneret to form a lumen. The air gap for the spinning process is 10 cm. During the spinning process, the membrane produced was allowed to immerse in the water as an external coagulant bath for 24 h to complete the phase-inversion process. The membrane was then cut into the same length around 30 cm each and dried at room temperature for another 24 h. Then, the alumina hollow fiber membranes were sintered at 1400 °C in a tubular furnace (XL-1700) started from room temperature to 400 °C at a rate of 3 °C min^{-1} and held for 1 h. The heating process was further continued at 800 °C with the heating rate of 4 °C min^{-1} and held for 2 h. The sintering temperature was fixed at 1400 °C, held for 8 h at the temperature rate of 5 °C min^{-1}. Finally, the sintering process was completed when the target temperature was cooled down to room temperature at a rate of 5 °C min^{-1}.

2.3. Preparation of ZIF-8 membrane

2.3.1. 3-(aminopropyl)triethoxysilane (APTES) modification on alumina hollow fiber membrane

APTES modification on the alumina hollow fiber membrane support was done according to the previous method with slight modification [28]. First, the alumina hollow fiber membrane was sonicated in acetone, methanol and deionized water for 5 min. The cleaned alumina hollow fiber membranes were then silanized with 2% APTES solution in toluene for 2 h. After the reaction, the modified membrane was washed with ethanol and dried. The solvent on the membrane's surface was removed by heating the membranes in the oven for 30 min at 60 °C before proceeded to the solvothermal growth of ZIF-8.

2.3.2. In situ solvothermal preparation of ZIF-8

APTES-modified and unmodified alumina hollow fiber membrane were fully immersed in the precursors' solution containing 2-methylimidazole, sodium formate and zinc nitrate hexahydrate with the molar ratio of 0.65 HCOONa: 1.0 $Zn(NO_3)_2$: 1.5 Hmim: 450 DMF in a Teflon bottle. The solution was heated at 120 °C for 24 h, 48 h and 72 h. The resulting membranes will be washed with methanol and dried at 60 °C for 24 h. The membrane without APTES modification is denoted as ZNA24, whereas the APTES modified membranes are denoted as ZA24, ZA48 and ZA72. For the ZIF-8 membranes prepared via the layer-by-layer method, the modification method was executed according to the method reported by Nagaraju et al. with slight modification [29]. The APTES modified membranes were first soaked in the Teflon bottle containing 2-Hmim solution and heated at 120 °C for 6 h. The membranes were then collected and soaked in the fresh solution mixture of zinc nitrate hexahydrate and sodium formate in another Teflon bottle. The bottle was heated in an oven at 120° for another 6 h. The procedures were repeated for 1 cycle and 2 cycles and the membranes denoted as Cycle 1 and Cycle 2 respectively. Fig. 1 illustrated the general synthesis of ZIF-8 on alumina hollow fiber membrane in the presence of APTES as the organic linker.

2.4. Characterizations

The surface and cross-section morphology of alumina ceramic membrane was viewed using a Scanning electron microscope (SEM) (Hitachi). A sample with 3 mm length was placed on a stab before being coated with platinum under vacuum for 3 min at 20 Ma (QUORUM). The alumina membrane's pore size distribution was measured using Mercury Porosimeter (Micrometrics AutoPore IV 9500). The crystallinity of ZIF-8 membranes was determined using X-ray diffractometer D5000 with CuKα radiation with a wavelength of 0.15406 nm at 40 kV

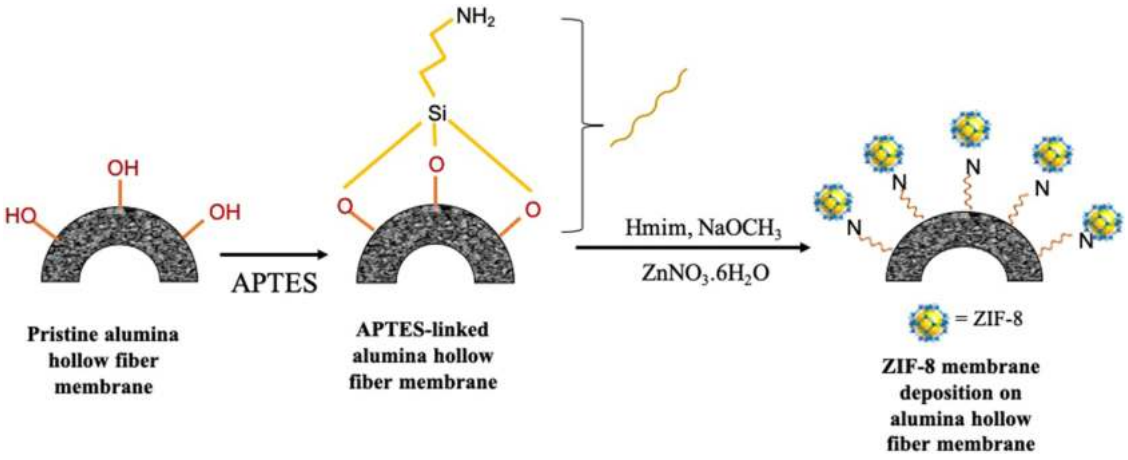

Fig. 1. General synthesis scheme for ZIF-8 membrane preparation.

and 40 mA. The step speed of 2°/min, ranging from 5° to 40° was used to record the samples XRD patterns. The presence of important ZIF-8 peaks was determined using Fourier Transform Infrared Spectroscopy (FTIR) analysis, recorded using Shimadzu IR Tracer-100 operating in transmittance mode. The morphology images of the ZIF-8 membranes were obtained using JEOL JSM-7600F field emission scanning electron microscope (FESEM) at an acceleration voltage of 2 kV.

2.5. Batch Adsorption Study

For copper(II) adsorption study, batch adsorption experiments were carried out by soaking 0.20 g of the membrane with 50 mL of copper(II) ion solutions at pH 6 for 6 h at room temperature, shaken at 150 rpm. The metal ion concentration was analyzed by UV–visible spectrophotometer (Lambda 25) at a wavelength of 275 nm, using polyethyleneimine (PEI) as reported by a previous study [30]. The percentage of copper(II) removal and adsorption capacity of the membrane was calculated using Eq. (1) and Eq. (2) respectively.

$$Cu(II)removal \quad (\%) = \frac{C_o - C_e}{C_o} \times \quad 100 \tag{1}$$

$$q_e = \frac{(C_o - C_e)V}{m} \tag{2}$$

Where C_o(mg/L) refers to the initial and C_e refers to the final concentration of copper(II) ion, m is mass of the adsorbent, and V is the volume of copper(II) solution.

Evaluation of the sorption mechanism was carried out based on Langmuir and Freundlich isotherms. The Langmuir isotherm applies to adsorption on completely homogeneous surfaces with negligible interaction between adsorbed molecules. Meanwhile, the Freundlich isotherm can be applied for heterogeneous surfaces and multilayer sorption. Eqs. (3) and (4) represents Langmuir and Freundlich, respectively.

$$\frac{C_e}{q_e} = \frac{C_e}{q_m} + \frac{1}{bq_m} \tag{3}$$

$$q_e = K_F C_e^{1/n} \tag{4}$$

Where,

C_e = equilibrium concentration (mg/L)
q_e = adsorption capacity at equilibrium (mg/g)
q_m = maximum adsorption capacity of the adsorbent (mg/g)
b = Langmuir adsorption constant
K_F = Freundlich adsorption constant
n = heterogeneity factor

Then, the evaluation of the reaction orders based on the adsorbent's capacity was carried out using first-order and second-order of adsorption kinetics as shown in the Eqs. (5) and (6), respectively.

$$\ln(q_e - q_t) = lnq_e - k_1 t \tag{5}$$

$$\frac{t}{q_t} = \frac{1}{k_2 q_e^2} + \frac{1}{q_e} t \tag{6}$$

Where,

q_e = adsorption capacity at equilibrium (mg/g)
q_t = adsorption capacity at time (mg/g)
t = time (min)
k_1 = equilibrium constant for first-order
k_2 = equilibrium constant for second-order

2.6. Filtration study

2.6.1. Permeate and copper(II) rejection

A cross-flow filtration system was used to determine the solute permeate and rejection of copper(II). Firstly, the feed solution was pumped into the outer side of the hollow fiber membrane, allowing the water to penetrate to the membrane's inner side. The solution then flows through the lumen to the other unsealed end of the hollow fiber membrane. The system's trans-membrane pressure is fixed at 1 bar, and the process was run at room temperature. The permeates was stabilized for about 30 min before being collected for flux and rejection determination. Fig. 2(a) is the cross-flow system diagram whereas the Fig. 2(b) is the specification of the hollow fiber module. The solute flux was calculated using Eq. (7) [31].

$$J_w = \frac{V}{t \quad \times \quad A} \tag{7}$$

Where, J_w = Solute flux.

V = volume of permeate (m^3),
t = time of permeate collected (h)
A = total surface area of hollow fibre membrane (m^2)

For copper(II) filtration study, copper(II) sulfate ($CuSO_4$) solution with the concentration of 10 ppm was used. The percentage of copper (II) removal was also determined by using Eq. (1).

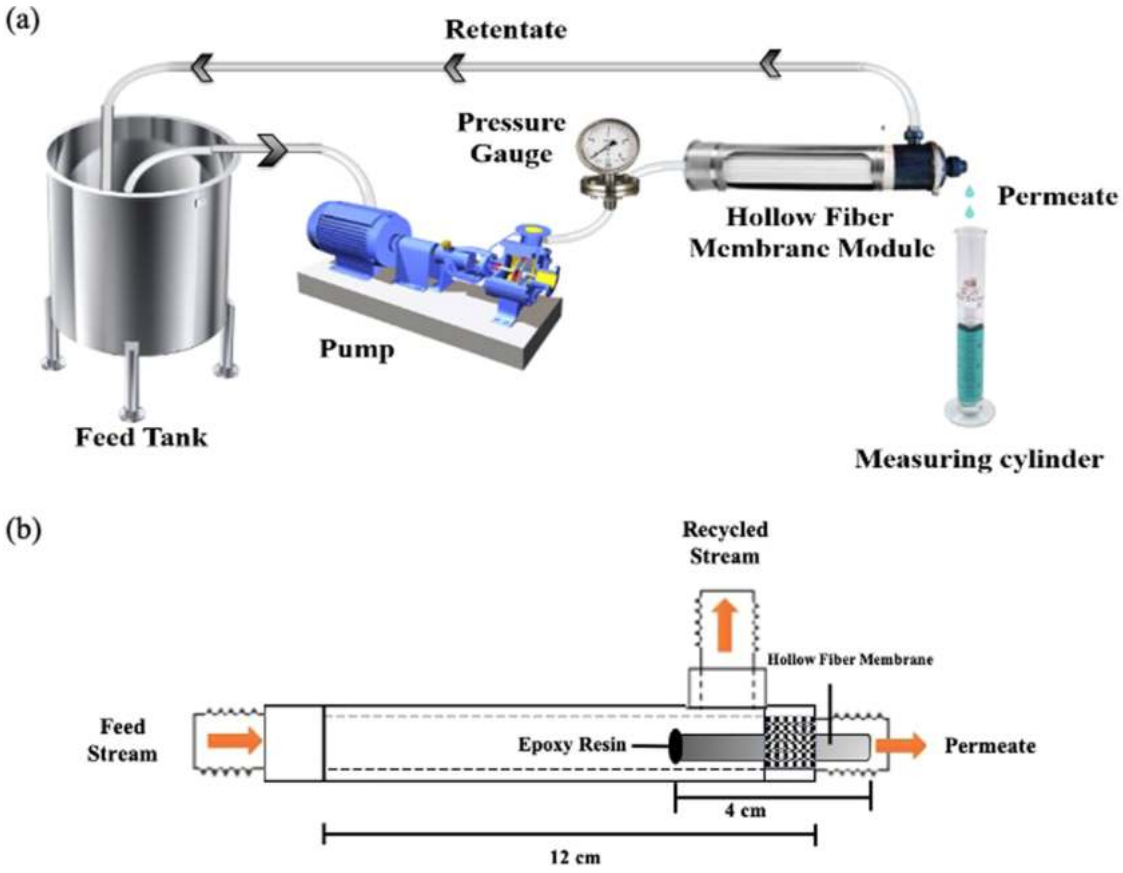

Fig. 2. (a) Cross-flow filtration system set up (b) specification of the hollow fiber module.

3. Results and discussion

3.1. Preparation of alumina hollow fiber membrane

Fig. 3 depicted the cross-section scanning electron image (SEM) and surface images of pristine alumina hollow fiber membrane prepared via phase-inversion and sintering method. The outer diameter of the membrane is 1.73 mm, and the inner diameter of the membrane is 1.03 mm. The thickness of the membrane in 0.70 mm. The SEM image showed that the membrane has a finger-like combination at the shell and lumen side of the membrane. The morphology can be attributed to the instantaneous demixing after the immersion of the precursor in the non-solvent bath [32]. The sponge-like structure in the middle of the hollow fiber membrane is attributed to the delayed demixing due to the longer precipitation process and the slow formation of the membrane. However, as shown in the SEM micrograph, a thin layer of sponge-like structures is on top of the large finger-like configuration. This morphology is an advantageous characteristic for the deposition of ZIF-8 layer on top of the membrane because the sponge-like structure comprises narrow pores. Therefore it can help to avoid the penetration of ZIF-8 particles into the inner part of the membrane.

The surface image of the alumina hollow fiber (Fig. 3b) also exhibited the membrane's high porosity. Mercury Intrusion Porosimetry (MIP) analysis was also conducted to determine the porosity of the alumina support. The results showed in Fig. 4 revealed that the membrane support comprises two distinct pore size diameter. The bigger

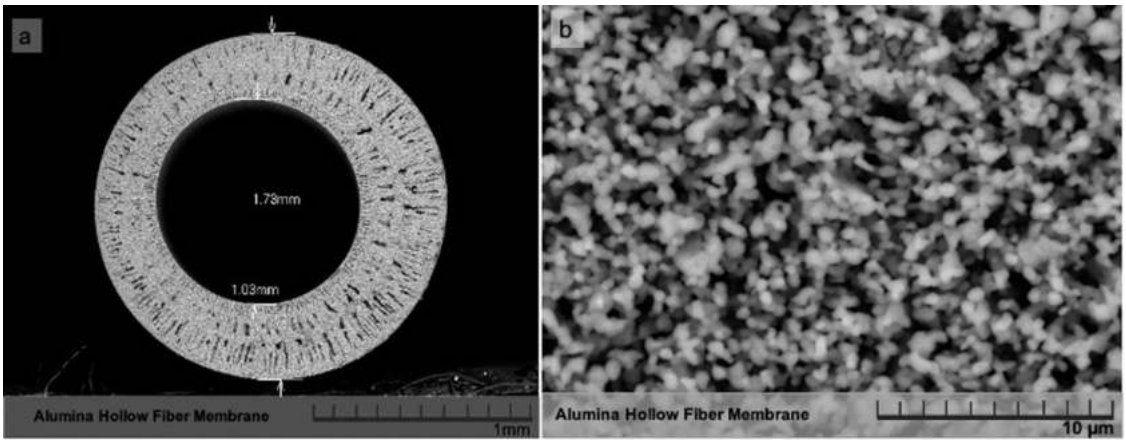

Fig. 3. SEM images of alumina hollow fiber (a) cross-section (b) surface.

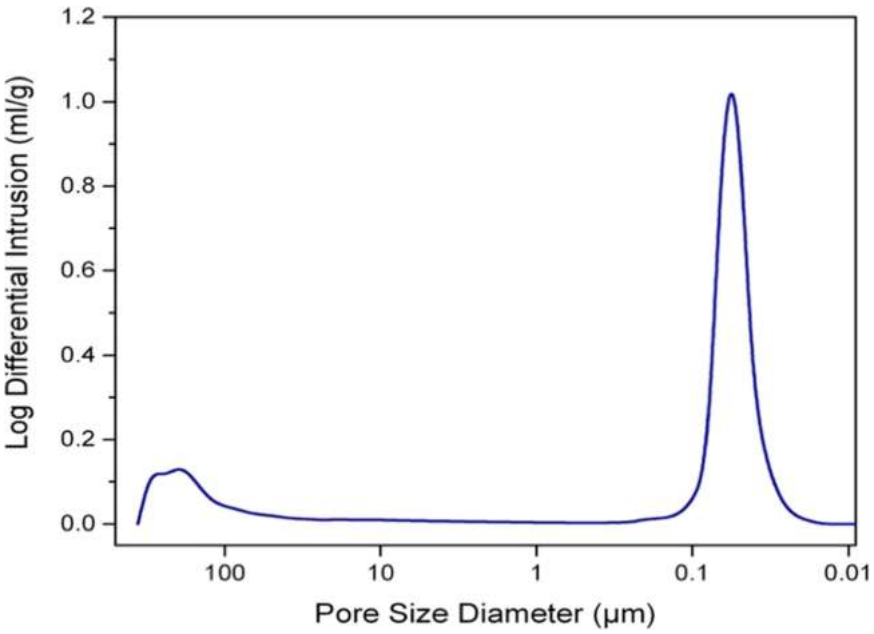

Fig. 4. Pore Size Distribution of Alumina Hollow Fiber Membrane Support.

diameter at around 100 μm represented the appearance of the finger-like structures. In contrast, the smaller pores around 0.01–0.1 μm signified the existence of the sponge-like structures. The MIP data also the porous structure of the alumina support membrane. Therefore, further modification on the surface of the support membrane is required to reduce the membrane's surface porosity to enhance the performance of the membrane for copper(II) ions removal.

3.2. Synthesis of ZIF-8 membrane on alumina hollow fiber membrane

The presence of functional groups in ZIF-8 membranes was analyzed using FTIR and shown in Figs. 5 and 6. Fig. 5 compared the functional group existed in the ZIF-8 membrane prepared with APTES and without the presence of APTES. The intense band observed for ZIF-8 alumina hollow fiber membrane with APTES modification revealed the formation of ZIF-8 layer on the alumina support. The C=N stretching was identified at 1589 cm^{-1}, whereas the peak at around 1380 cm^{-1} attributed to the entire ring stretching fingerprint. Several bands were also observed in the range of 1350–900 cm^{-1}, associated with the presence of in-plane bending of the ring and the bands around 750–690 cm^{-1} correlated to the existence of aromatic sp^2 C–H bending. The Zn-N stretching can be observed at a wavenumber of around 450 cm^{-1}.

On the other hand, the ZIF-8 membrane prepared without APTES modification showed no apparent ZIF-8 bands at the IR region, indicating that the formation of ZIF-8 membrane on top of the alumina support is not well-grown or in traces amount. Fig. 6 compares the FTIR spectra for all the prepared membrane with APTES modification. The band intensity increase when the duration of synthesis for *in situ* solvothermal synthesis increase from 24 h to 72 h. The FTIR transmittance bands showed that the ZIF-8 layer was successfully formed on top of the

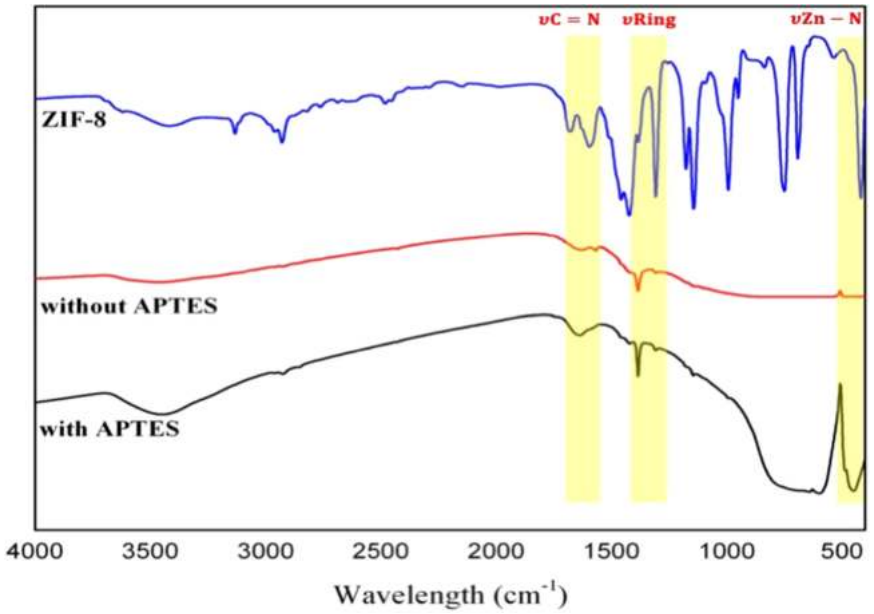

Fig. 5. FTIR spectrum for ZIF-8 prepared with APTES and without APTES modification.

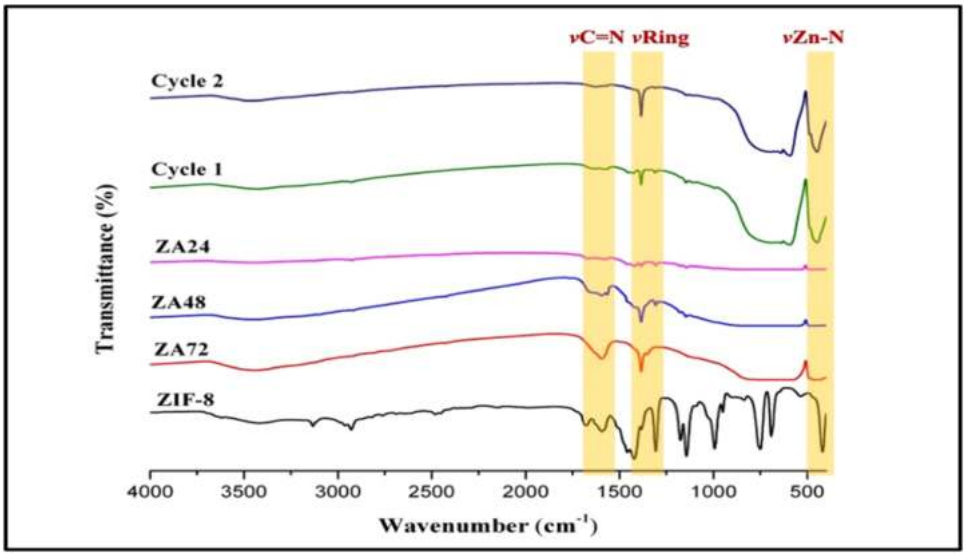

Fig. 6. FTIR spectra of all the prepared membranes.

alumina support for the membrane prepared via the layer-by-layer technique. Noticeably, the intensity of the bands intensifies with the increase in the number of cycles performed.

The XRD data obtained is shown in Fig. 7 and Fig. 8. By referring to Fig. 7, the XRD peaks for ZIF-8 growth on APTES modified alumina membranes were in good agreement with previous reports, thus confirming the formation of pure crystalline ZIF-8 phase [33,34]. While for the unmodified alumina surface, the growth of ZIF-8 on top of the membrane seems to be unsuccessful because the presence of ZIF-8 can only be detected as traces. As expected, the APTES modified alumina membrane showed the characteristic reflection of ZIF-8 at $2\theta = 7.30$, 10.35, 12.70, 14.80, 16.40 and 18.00°, attributed to the (110), (200), (211), (220), (310), and (222) planes, respectively [35]. All the membranes with APTES modification, prepared at different reaction time also showed the same characteristic reflection. The ZA72 showed the highest intensity, indicating that the longer reaction time produced ZIF-8 membrane with a better crystalline structure. While for membrane prepared via layer-by-layer, the membranes show the characteristic reflection of ZIF-8 peaks, but with rather lower intensity than the prior method as shown in Fig. 8. By comparing the intensity of 1 cycle membrane and the 2 cycles membrane, the 2 cycles membrane has more intense XRD peaks than the 1 cycle membrane. Therefore, it is noted that the number of cycles affects the peak intensity of the XRD peak of the ZIF-8 membrane [36]. The increase in the number of cycles is expected to increase the possibility of forming more ZIF-8 crystals because the chances of the precursors to react with each at the second cycle are higher than the single cycle. The higher intensity in second cycle membrane indicated the higher deprotonation of 2-methylimidazole

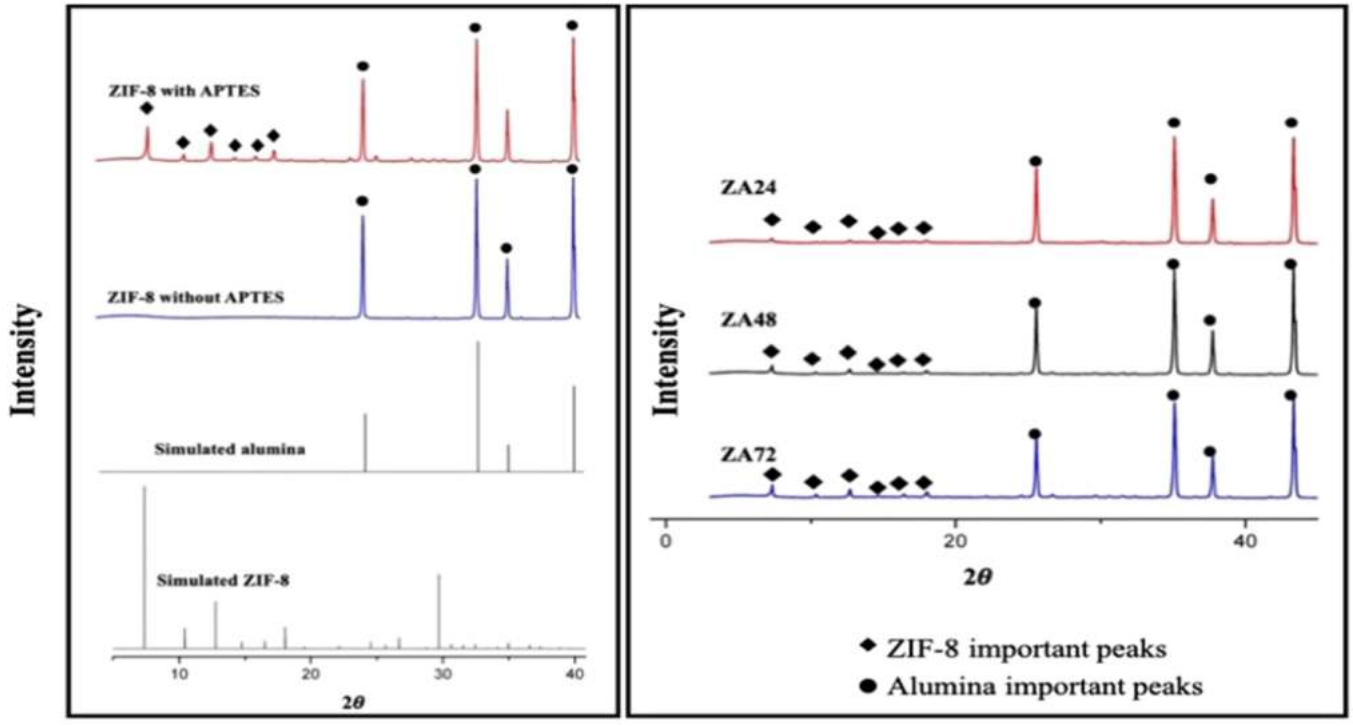

Fig. 7. XRD peaks of ZIF-8 and ZA24, ZA48 and ZA72 membranes.

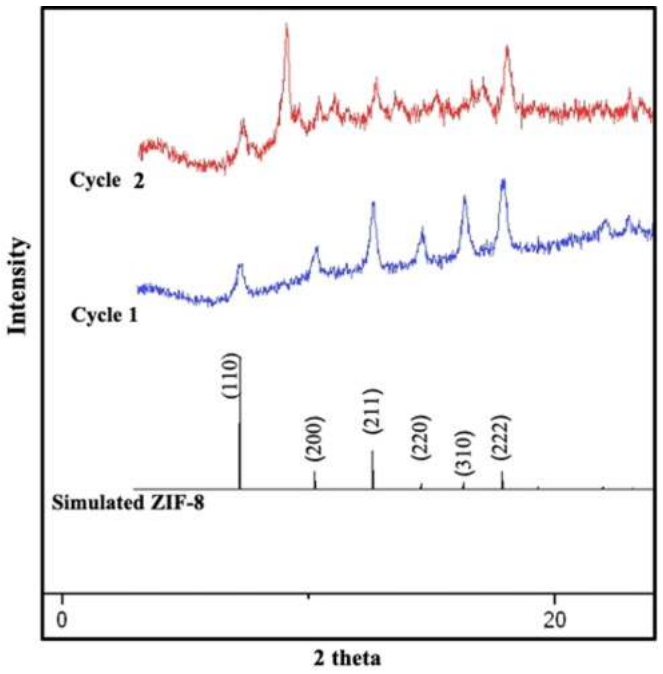

Fig. 8. The XRD spectrum of Cycle 1 and Cycle 2 ZIF-8 membrane compared with the *simulated ZIF-8 data*.

[37] and the formation of ZIF-8 with better crystallinity and better coverage [38]. Better coverage of ZIF-8 on the membrane gives chances for more adsorption sites for copper(II) ions and enables the ions' filtration better than the not-fully covered membrane. ZIF-8 with high crystallinity also tends to be stable rather than the low crystallinity structure. The high crystalline structure also indicates the good formation of ZIF-8 crystal membrane with fewer guest molecules in the crystal structure [35]. If the guest molecules in the crystal framework are absent, the chance for copper(II) adsorption is higher, thus improving the copper(II) removal.

Fig. 9 shows the FESEM images of ZIF-8 membranes prepared via a solvothermal method at a different time of synthesis and ZIF-8 membrane prepared via layer-by-layer techniques. Fig. 8a(i) and (ii) is the morphology of ZIF-8 growth on the non-modified alumina substrate. The FESEM images reveal that the membrane prepared without the APTES modification formed layer with no rhombic dodecahedron shape. On the other hand, the ZIF-8 membranes prepared with the APTES modification has the rhombic dodecahedron shape. The rhombic dodecahedron shape is reported to be the stable equilibrium morphology of ZIF-8 [39]. A study by Linder-Patton et al. revealed that the dodecahedron shape has a more active site for adsorption than the cube shape of ZIF-8 particles [40]. The APTES enables better growth of ZIF-8 on the surface of alumina hollow fiber membrane because APTES can effectively enhance the heterogeneous nucleation of the ZIF-8 crystals [41]. Besides, the APTES modified alumina hollow fiber membrane can enhance the surface hydrophobicity of the alumina membrane. Therefore, the hydrophobic property of ZIF-8 membrane tends to grow well on the hydrophobic surface, just like the "like grows like" principles [42].

Duration of synthesis also plays a vital role in determining the shapes of the ZIF-8 formed during the synthesis. In can be seen from the Fig. 8b (i), b(ii), c(i), c(ii), d(i) and d(ii), the ZIF-8 crystals prepared at synthesis time of 24 h has the thinnest layer of ZIF-8 membranes whereas the ZA72 has the thickest layer among all. Apart from that, the crystal size of ZIF-8 also observed to be increased by increasing the reaction time. Whilst, for Cycle 1 and Cycle 2, the layer has no obvious crystal shape with thin layer but more compact compared to the membranes prepared via *in situ* solvothermal methods.

3.3. Adsorption study of copper(II)

3.3.1. Effect of pH on copper(II) removal

The pH of copper(II) solution is one of the important factors affecting the adsorption capacity and the removal efficiency of copper(II) in a solution due to the ability of pH to influence the structural stability and the surface charge of the adsorbent [19]. Fig. 10 described the effect of pH on the copper(II) adsorption on ZA24, ZA48 and ZA72 at pH 5 to pH 8. The results denoted that, all the membranes exhibited the highest capability of adsorption at pH 6. Among the three membranes, ZA72 showed the highest copper(II) removal. The high removal of copper(II) might be related to the higher thickness of the ZIF-8 layer of the membrane compared to other membranes. Several studies proved that the thicker MOF membrane has higher adsorption capability than the thinner membrane [43,44]. The thicker membranes have more adsorption sites due to the higher amount of adsorbents.

The figure also implied that the removal of copper(II) reduces with the increase of pH value. At pH 5, the adsorption percentage is low due to the competitive factor between H^+ and Cu^{2+} for the adsorbents' exchange site [45]. The membranes showed highest adsorbance capacity at pH 6; however, the adsorption on membranes decreases when the pH increase to pH 7 and 8. This phenomenon is due to the precipitation of copper(II) ion at pH higher than pH 6 [46].

3.3.2. Batch Adsorption Study

Table 1 shows the data for the adsorption study of copper(II) ions on ZIF-8 membranes which includes the isotherms and kinetic study. The adsorption test was carried out at pH 6, at the concentration range of 20–100 ppm for 6 h. The data indicated that copper(II) 's adsorption mechanism was best fitted the Freundlich model with the R^2 value of 0.9436 compared to the Langmuir model with the R^2 of 0.53717. The Freundlich model inferred that the copper(II) ions adsorbed on the heterogeneous surface by multilayer adsorption [47], while the slope ($1/n$) indicated that the adsorption intensity or surface heterogeneity of the adsorbents. The surface is more heterogeneous if its value reaches closer to zero [48]. The data of this adsorption study, the $1/n = 0.85$, denotes the ZIF-8 membrane surface's less heterogeneity. On the other hand, n describes the types of interaction involved during the adsorption process [49]. If $n > 1$, the adsorption involves chemical interaction whereas, if the $n < 0$ demonstrates the physical interaction occurred. If $n = 1$ means no adsorption process will occur. In this study, the value of $n = 1.179$, thus the interaction between copper(II) and ZIF-8 membrane could be designated as a chemisorption process. The Freundlich and Langmuir isotherm graph are shown in Fig. 11.

Pseudo-first order and pseudo-second-order model were used in this study to determine the adsorption mechanism of copper(II) on the ZIF-8 membrane. The correlation coefficient (R^2) indicated the conformity between experimental data and the model-predicted value. The kinetic data of pseudo-first-order and pseudo-second-order is shown in Table 1. The results indicated that the adsorption kinetics of the ZIF-8 membrane is better fitted the pseudo-second-order model rather than the pseudo-first-order model with the correlation coefficient (R^2) value of 0.9738. Hence it can be established that the adsorption of copper(II) ions on the ZIF-8 membrane perfectly follow the pseudo-second-order kinetic model. Additionally, the value of theoretical q_e from the pseudo-second-order model was close to the experimental value. In this model, the rate-limiting step was the surface adsorption, involving chemisorption, where the removal from a solution is due to physicochemical interactions between two phases [50]. The graph for pseudo-first-order and pseudo-second-order graph are shown in Fig. 12.

According to Zhang et al. the removal of copper(II) on ZIF-8 involves the ion exchange if the copper(II) solution concentration is below 200 ppm [19]. The adsorption mechanism is shown in Fig. 13. During the adsorption process, the zinc(II) ion in ZIF-8 framework is replaced by copper(II), thus forming a new complex. The phenomenon is due to the similar atomic radius of zinc and copper ion. The electron layer of zinc is

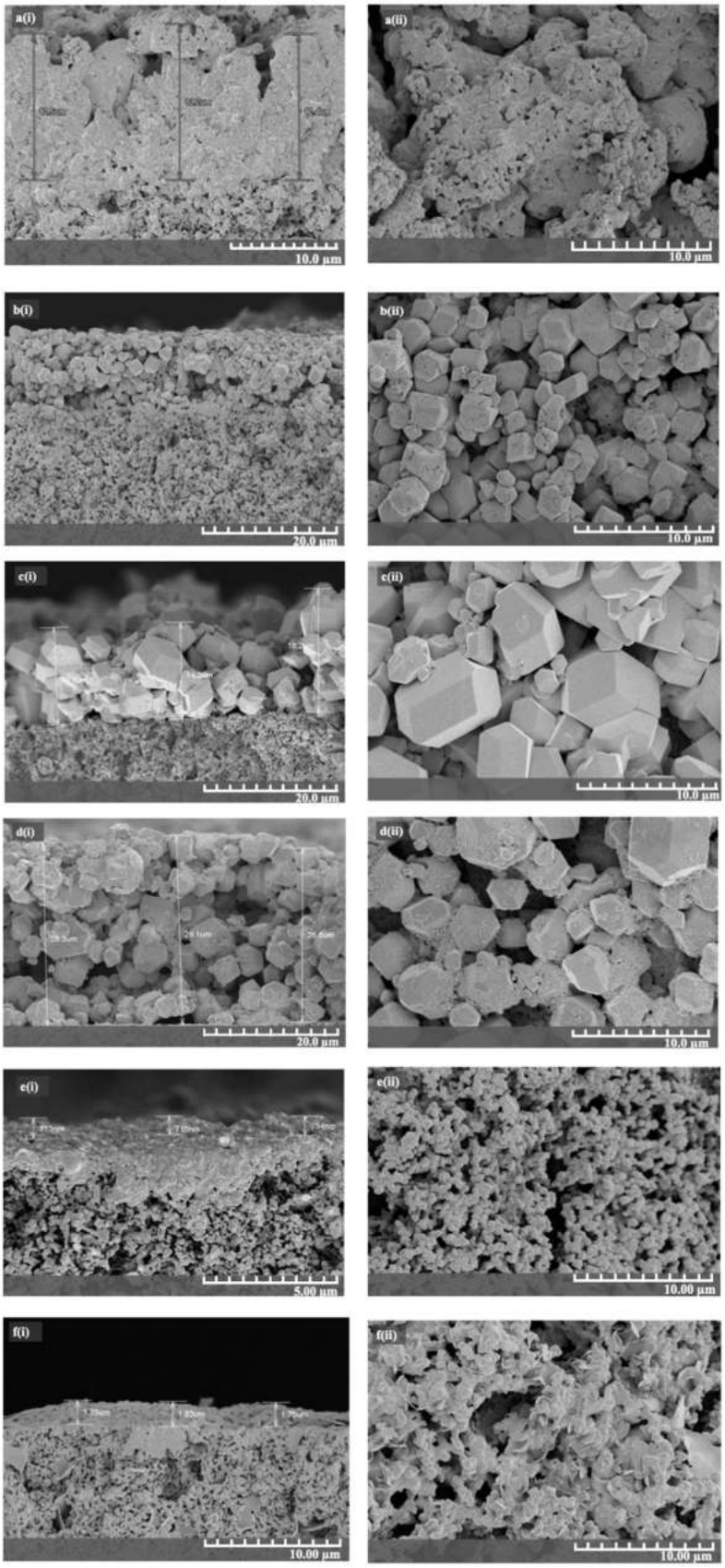

Fig. 9. FESEM images of a(i) ZNA cross-section a(ii) ZNA surface b(i) ZA24 cross-section b(ii) ZA24 surface c(i) ZA48 cross-section c(ii) ZA48 surface d(i) ZA72 cross-section d(ii) ZA72 surface e(i) Cycle 1 cross-section e(ii) Cycle 1 surface f(i) Cycle 2 cross-section f(ii) Cycle 2 surface.

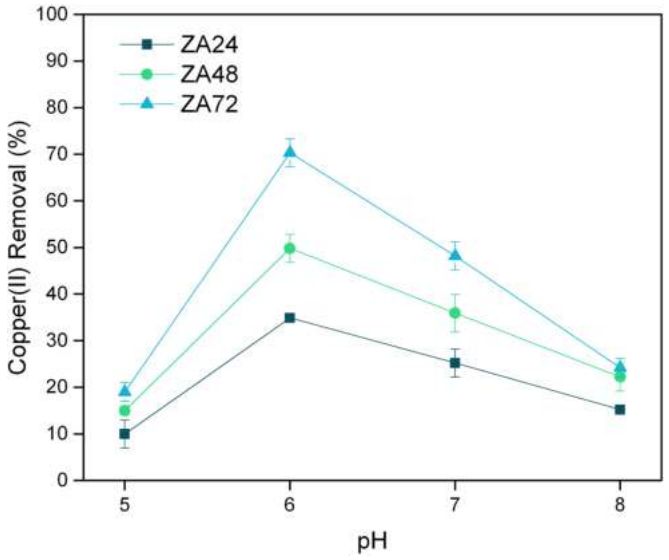

Fig. 10. The effects of pH on copper(II) removal.

Table 1
Adsorption isotherm and kinetic study data.

Adsorption Isotherm			
Langmuir Model	q_m	k_L	R^2
	2.68×10^2	0.0102	0.53717
Freundlich Model	N	k_F	R^2
	1.1719	3.4171	0.94363
Kinetic Study	q_e *(exp)*	76.5 mg/g	
First Order	q_e	k_1	R^2
	39.64 mg/g	0.00267	0.8777
Second Order	q_e	k_2	R^2
	65.32 mg/g	0.0276	0.97382

more stable than copper, thus making the coordination of copper complexes stronger than the zinc complexes.

3.4. Filtration study

The performance of ZIF-8 membranes was further determined by conducting the filtration process using a cross-flow filtration system at 1 bar. The membrane's performance in terms of the results of copper(II) ion removal capacity and water flux is demonstrated in Fig. 14. The pristine membrane showed the highest flux among all tested membranes with almost 700 Lm $^{-2}$h^{-1}. However, the pristine membrane unable to reject the copper(II) ions. This phenomenon is due to the high porosity of the membrane and the average pore size, which are bigger than the copper(II) ions, as signified by the MIP data discussed earlier. Whilst, among all of the ZIF-8 membranes, the ZA24 membranes exhibited the highest flux among all, with almost 500 Lm^{-2}h^{-1}, but only rejected about 30% of the copper(II) ions. The result is due to the porous structure of the ZA24 compared to the other ZIF-8 membranes as can be seen from the FESEM images. The high porosity leads to less copper(II) ions rejection and also highest flux among all. The ZA48 and ZA72 showed an increase in copper(II) rejection but a significant flux decrease. The difference in membrane thickness is believed to be the possible reason for the membranes' different performance because thick membranes have higher resistance and restrict water pathway across the membranes [34].

On the other hand, membrane prepared via layer-by-layer technique demonstrated the highest rejection, with the copper(II) rejection of 90% but with the lowest flux (133 Lm^{-2}h^{-1}). The results can be related to the compact and dense structure of the ZIF-8 layer formed on the alumina support. Dense layer on top of the membrane plays important roles in the membranes' selectivity [51]. The dense layer also provides better mass transfer resistance to the membrane, thus improving the rejection of copper(II) ions better than other prepared membranes with a more porous structure. From the results obtained, the relationship between flux and copper(II) rejection is inversely correlated. The porosity and thickness of membrane play a vital role in determining the trade-off effect. The dense and compact membrane is undoubtedly exhibited higher ions rejection performance, but the low water flux exhibited is also not favourable. Therefore, to achieve high water flux, the pore size of ZIF-8 membranes must be controlled so that the membrane can retain

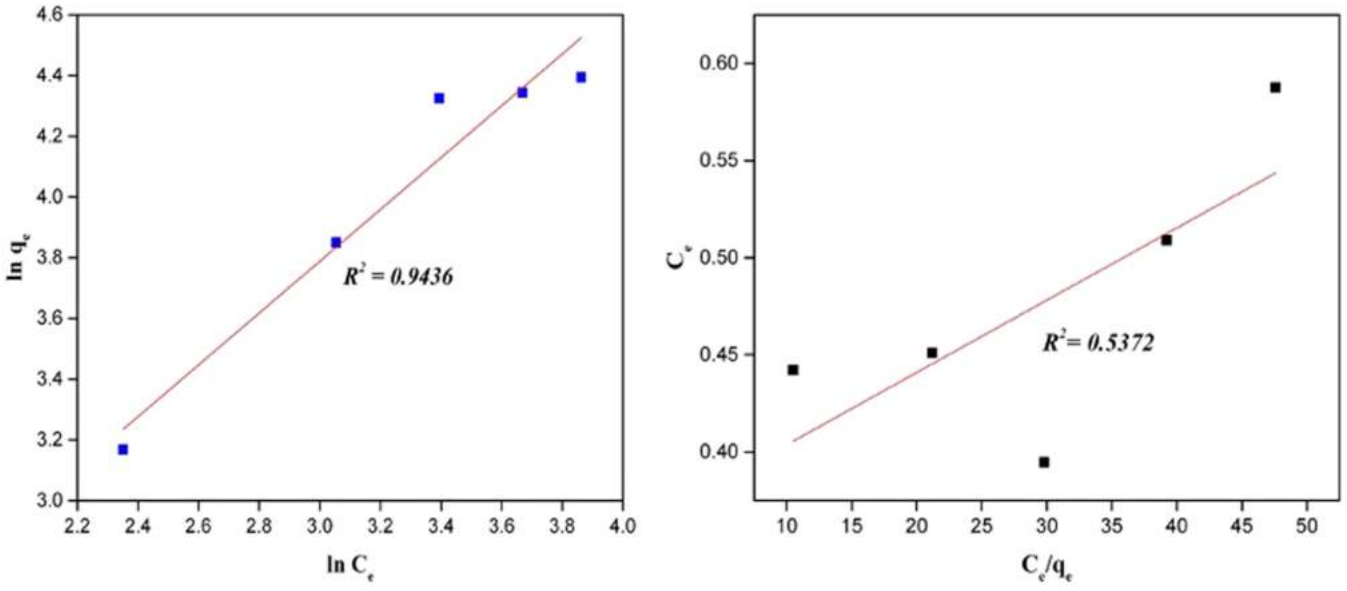

Fig. 11. The Freundlich and Langmuir plot of copper(II) adsorption.

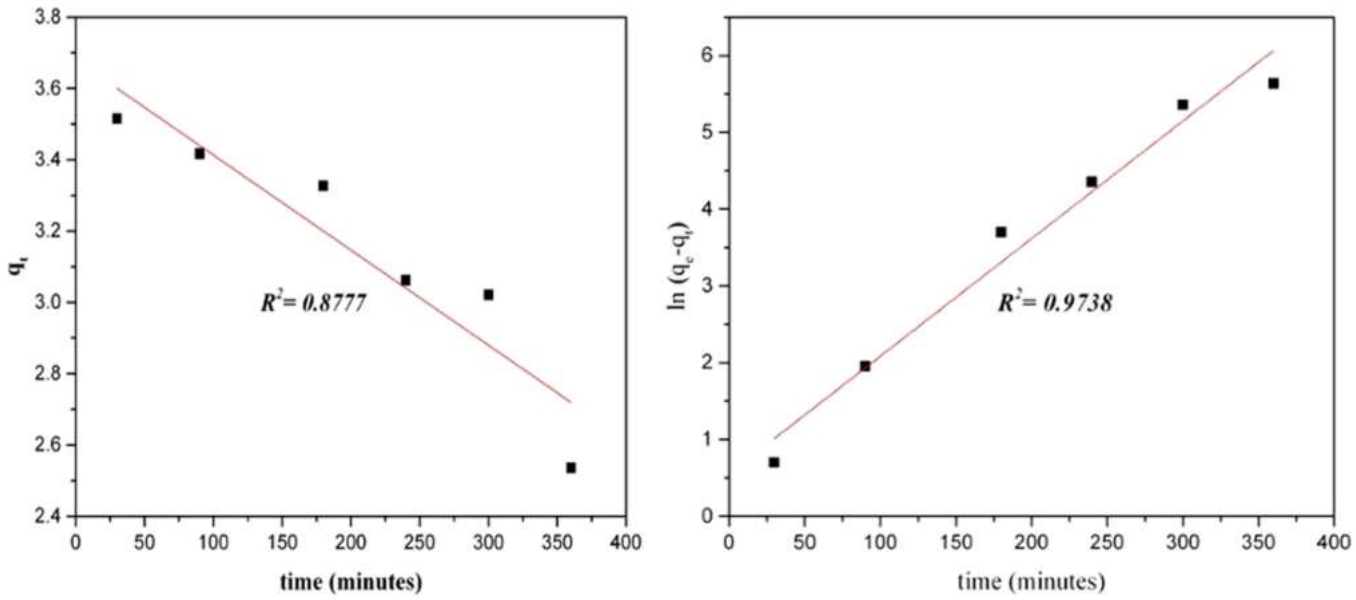

Fig. 12. The pseudo-first-order and pseudo-second-order kinetic model for copper(II) removal on ZIF-8 membrane.

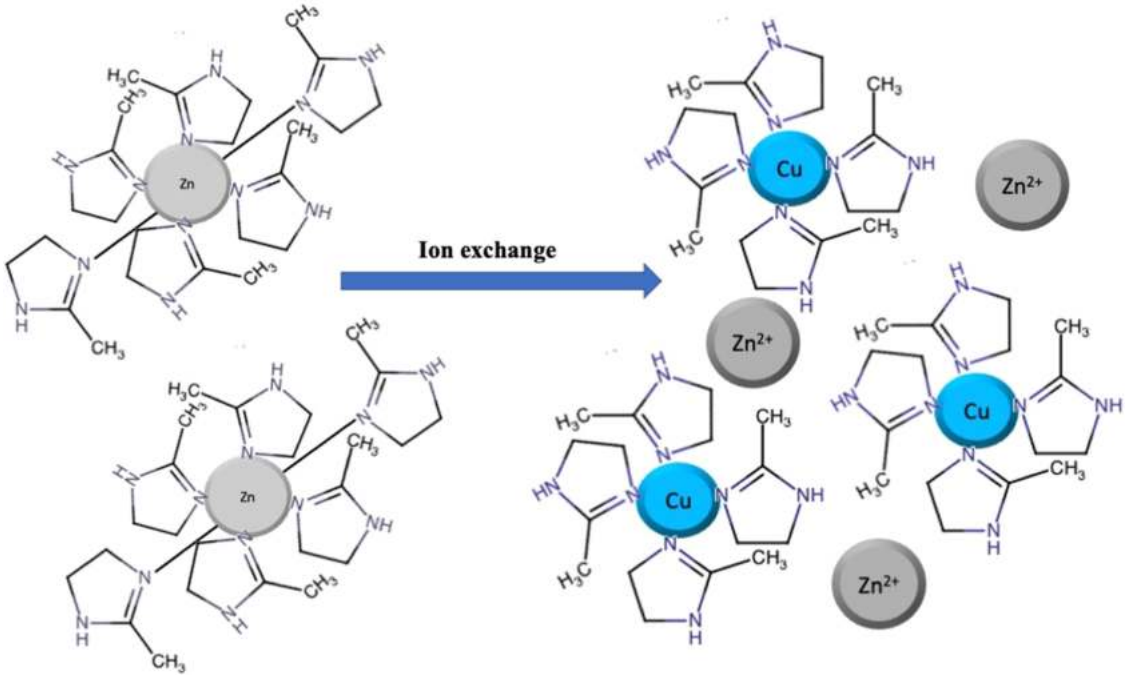

Fig. 13. The adsorption mechanism of copper(II) ions by ZIF-8 membrane.

the copper(II) ions to pass through the membranes, without restricting the water to pass through. The membranes' thickness also needs to be controlled to reduce the water pathway resistance across the membranes. Table 2 compares the previous related study on the use of ceramic-based adsorptive membrane for copper(II) removal.

4. Conclusion

The ZIF-8 membranes were successfully prepared via *in situ* solvothermal method and layer by layer method with APTES as the linker. The APTES modification on alumina support exhibited a significant effect on the formation of ZIF-8 layer on the alumina support. ZIF-8 membranes prepared via *in situ* solvothermal method have higher crystallinity than the membranes prepared via layer by layer method. Besides, the increasing duration of the in situ solvothermal method's reaction time produced thicker ZIF-8 membrane with almost the same crystal structure compared to the shorter synthesis time membrane. Batch adsorption study of copper(II) on ZIF-8 membrane revealed that the adsorption mechanism is well fitted with the Freundlich and pseudo-second-order model for the isotherm and kinetic study, respectively. The copper(II) ion solution's filtration can remove up to 90% of the copper (II) ions with the flux of 133 $Lm^{-2}h^{-1}$. In conclusion, copper(II) ions can be instantaneously removed by the ZIF-8 hybrid membrane via adsorption and filtration, therefore becoming a promising potential for future heavy metal wastewater treatment application.

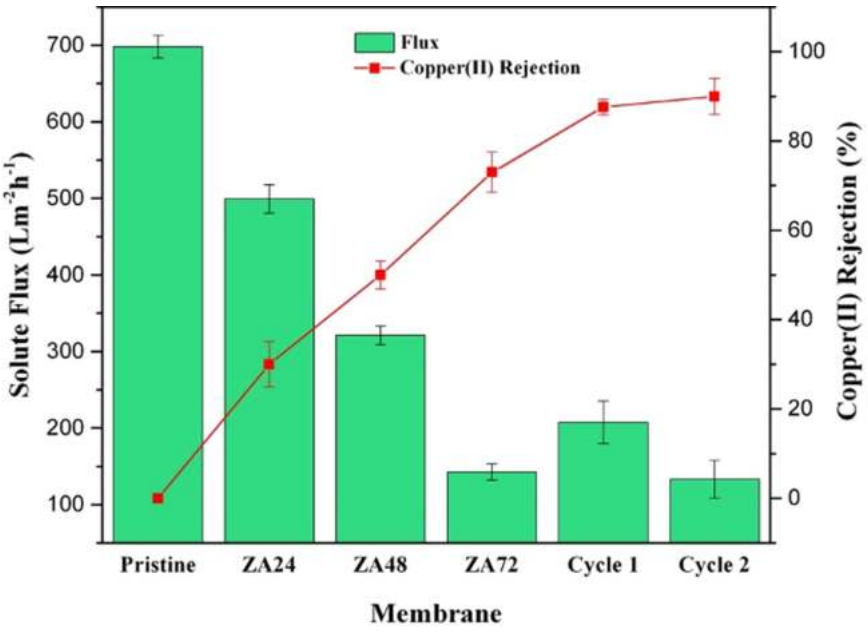

Fig. 14. The solute flux and copper(II) rejection of ZIF-8 membranes.

Table 2
Comparison of ceramic-based/materials adsorptive membrane for copper(II) removal.

Types of membrane	Adsorption capacity (q_{max})	Flux	Rejection (%)	References
Chitosan oxidized-CNT in pore channel of alumina ceramic support	7.04	23.45 kg/m^2h	76.76	[52]
Ceramic membranes containing a mixture of local clay and sawdust (dimensions: 15 cm × 15 cm × 2 cm)	Not mentioned	Not mentioned	99	[53]
Mixed matrix membrane (PES added with alumina nanoparticles)	14	Not mentioned	66	[54]
γ-alumina coated on Ppy membrane	20.6	Not mentioned	81	[55]
PSf added with:				
(i) Bentonite	1.0	46 $Lm^{-2}h^{-1}$	59.2	[56]
(ii) Sepiolite	0.29	144 $Lm^{-2}h^{-1}$	21.5	
(iii) Zeolite	2.82	126 $Lm^{-2}h^{-1}$	97.0	
ZIF-8 membranes on alumina hollow fiber support	76.5	133 $Lm^{-2}h^{-1}$	90	Present study

CRediT authorship contribution statement

Dayang Norafizan binti Awang Chee: Conceptualization, Methodology, Investigation, Data curation, Visualization, Writing - original draft. **Ahmad Fauzi bin Ismail:** Supervision, Funding acquisition. **Farhana Aziz:** Supervision, Writing - review & editing. **Mohamed Afizal Mohamed Amin:** Data visualization, Writing - original draft. **Mohd. Sohaimi Abdullah:** Resources.

Declaration of Competing Interest

The authors declare that they have no known competing financial interests or personal relationships that could have appeared to influence the work reported in this paper.

Acknowledgement

The authors gratefully acknowledge financial support from the Ministry of Higher Education through the Higher Institution Centre of Excellence (HICoE) (R.J090301.7809.4J424). Appreciation also goes to UTM Research Management Centre for both financial and technical support.

References

[1] J. Briffa, E. Sinagra, R. Blundell, Heavy metal pollution in the environment and their toxicological effects on humans, Heliyon 6 (2020), e04691, https://doi.org/10.1016/j.heliyon.2020.e04691.
[2] H. Services, Toxicological Profile for Copper, 2004. doi:10.1201/9781420061888_ch123.
[3] K. Simeonidis, S. Mourdikoudis, E. Kaprara, M. Mitrakas, L. Polavarapu, Inorganic engineered nanoparticles in drinking water treatment: a critical review, Environ. Sci. Water Res. Technol. 2 (2015) 43–70, https://doi.org/10.1039/C5EW00152H.
[4] A.R. Lucaci, D. Bulgariu, M.C. Popescu, L. Bulgariu, Adsorption of Cu(II) ions on adsorbent materials obtained from marine red algae Callithamnion corymbosum sp, Water 12 (2020) 372, https://doi.org/10.3390/w12020372.
[5] M. Bilal, J.A. Shah, T. Ashfaq, S.M.H. Gardazi, A.A. Tahir, A. Pervez, H. Haroon, Q. Mahmood, Waste biomass adsorbents for copper removal from industrial wastewater-a review, J. Hazard. Mater. 263 (2013) 322–333, https://doi.org/10.1016/j.jhazmat.2013.07.071.
[6] L. Lin, G. Liu, W. Lv, K.Y. Qintie Lin, Y. Zhang, Removal of chelated copper by TiO2 photocatalysis: synergetic mechanism between Cu (II) and organic ligands, Iran. J. Chem. Chem. Eng. 32 (2013) 103–112.
[7] I.A. Khattab, M.F. Shaffei, N.A. Shaaban, H.S. Hussein, S.S. Abd El-Rehim, Electrochemical removal of copper ions from dilute solutions using packed bed electrode. Part I, Egypt. J. Pet. 22 (2013) 199–203, https://doi.org/10.1016/j.ejpe.2012.09.011.
[8] T.A. Kravchenko, L.L. Polyanskiy, V.A. Krysanov, E.S. Zelensky, A.I. Kalinitchev, W.H. Hoell, Chemical precipitation of copper from copper-zinc solutions onto selective sorbents, Hydrometallurgy 95 (2009) 141–144, https://doi.org/10.1016/j.hydromet.2008.05.027.
[9] M.M. Brbooti, B. a Abid, N.M. Al-shuwaiki, Removal of heavy metals using chemicals precipitation, Engine Technol. J. 29 (2011).
[10] J.P. Bezzina, L.R. Ruder, R. Dawson, M.D. Ogden, Ion exchange removal of Cu(II), Fe(II), Pb(II)and Zn(II)from acid extracted sewage sludge – resin screening in weak acid media, Water Res. 158 (2019) 257–267, https://doi.org/10.1016/j.watres.2019.04.042.
[11] G. Bulut, U. Yenial, F. Goktepe, E. Albayrak, Removal of Copper from Waters by Ion Flotation Method, in: Proceedings of the Conf. Miner. Eng. Int. Conf. MEI, 2012.
[12] S.E. Ghazy, I.A. Mahmoud, A.H. Ragab, Removal of copper (II) from aqueous solutions by flotation using polyaluminum chloride silicate (PAX-XL60 S) as coagulant and carbonate ion as activator, Environ. Technol. 27 (2006) 53–61, https://doi.org/10.1080/09593332708618616.
[13] M.A. Barakat, New trends in removing heavy metals from industrial wastewater, Arab. J. Chem. 4 (2011) 361–377, https://doi.org/10.1016/j.arabjc.2010.07.019.

[14] R. Kumar, V. Prabhakar, J. Saini, Alumina, Int. J. Curr. Eng. Technol. 3 (2013) 1679–1685, https://doi.org/10.1016/0022-5193(72)90053-7.

[15] E. Jamieson, A. van Riessen, B. McLellan, B. Penna, C. Kealley, H. Nikraz, Introducing Bayer Liquor-Derived Geopolymers, Elsevier Inc, 2017, https://doi.org/10.1016/B978-0-12-804524-4.00008-7.

[16] J.H. Ha, S.Z. Abbas Bukhari, J. Lee, I.H. Song, C. Park, Preparation processes and characterizations of alumina-coated alumina support layers and alumina-coated natural material-based support layers for microfiltration, Ceram. Int. 42 (2016) 13796–13804, https://doi.org/10.1016/j.ceramint.2016.05.181.

[17] K.S. Park, Z. Ni, A.P. Côté, J.Y. Choi, R. Huang, F.J. Uribe-Romo, H.K. Chae, M. O'Keeffe, O.M. Yaghi, Exceptional chemical and thermal stability of zeolitic imidazolate frameworks, Proc. Natl. Acad. Sci. U. S. A. 103 (2006) 10186–10191, https://doi.org/10.1073/pnas.0602439103.

[18] P. Pillai, S. Dharaskar, S. Sasikumar, M. Khalid, Zeolitic imidazolate framework-8 nanoparticle: a promising adsorbent for effective fluoride removal from aqueous solution, Appl. Water Sci. 9 (2019) 1–12, https://doi.org/10.1007/s13201-019-1030-9.

[19] Y. Zhang, Z. Xie, Z. Wang, X. Feng, Y. Wang, A. Wu, Unveiling the adsorption mechanism of zeolitic imidazolate framework-8 with high removal efficiency on copper ions from aqueous solutions, Dalt. Trans. 45 (2016) 12653–12660, https://doi.org/10.1039/C6DT01827K.

[20] N. Wang, T. Liu, H. Shen, S. Ji, J.-R. Li, R. Zhang, Ceramic tubular MOF hybrid membrane fabricated through in situ layer-by-layer self-assembly for nanofiltratio, AIChE J. 62 (2016) 538–546, https://doi.org/10.1002/aic.

[21] Y.-S. Li, F.-Y. Liang, H. Bux, A. Feldhoff, W.-S. Yang, J. Caro, Molecular sieve membrane: supported metal-organic framework with high hydrogen selectivity, Angew. Chem. 122 (2010) 558–561, https://doi.org/10.1002/ange.200905645.

[22] K. Aylin, W. Lik H, P. Martin, B. Sara, A.M. Johan, V. Ivo F.J, Highly selective gas separation membrane using in situ amorphised metal–organic frameworks, Energy Environ. Sci. 10 (2017) 2342–2351, https://doi.org/10.1039/c7ee01872j.

[23] H. Zhang, W. Chen, K. Gong, J. Chen, Nanoscale Zeolitic Imidazolate Framework - 8 as Efficient Vehicles for Enhanced Delivery of CpG Oligodeoxynucleotides, 2017. doi: 10.1021/acsami.7b09583.

[24] Z.Q. Huang, Z.F. Cheng, Recent advances in adsorptive membranes for removal of harmful cations, J. Appl. Polym. Sci. 137 (2020) 48579, https://doi.org/10.1002/app.48579.

[25] K. Hu, K. Wang, J. Liu, Q. Dong, Hybrid membrane adsorbents: preparation and their adsorptions for copper(II) ions, Desalin. Water Treat. 57 (2016) 4606–4615, https://doi.org/10.1080/19443994.2014.1001442.

[26] S.A. Hamid, S.F. Azha, L. Sellaoui, A. Bonilla-Petriciolet, S. Ismail, Adsorption of copper (II) cation on polysulfone/zeolite blend sheet membrane: synthesis, characterization, experiments and adsorption modelling, Colloids Surf. A Physicochem. Eng. Asp. 601 (2020), 124980, https://doi.org/10.1016/j.colsurfa.2020.124980.

[27] N. Abdullah, M.A. Rahman, M. Ha, D. Othman, J. Jaafar, Preparation, characterizations and performance evaluations of alumina hollow fi ber membrane incorporated with UiO-66 particles for humic acid removal, 563, 2018, pp. 162–174. doi: 10.1016/j.memsci.2018.05.059.

[28] E.J. Sin, Y. Moon, Y.K. Lee, J. Lim, J. Huh, S. Choi, Y. Sohn, Surface modification of aluminium oxide for biosensing application, Biomed. Eng. Appl. Basic Commun. 24 (2012) 111–116, https://doi.org/10.1142/S1016237212500093.

[29] D. Nagaraju, D.G. Bhagat, R. Banerjee, U.K. Kharul, In situ growth of metal-organic frameworks on a porous ultrafiltration membrane for gas separation, J. Mater. Chem. A 1 (2013) 8828, https://doi.org/10.1039/c3ta10438a.

[30] T. Wen, F. Qu, N.B. Li, H.Q. Luo, A facile, sensitive, and rapid spectrophotometric method for copper(II) ion detection in aqueous media using polyethyleneimine, Arab. J. Chem. 10 (2017) S1680–S1685, https://doi.org/10.1016/j.arabjc.2013.06.013.

[31] D.N. Awang Chee, A.F. Ismail, F. Aziz, M.A. Mohamed Amin, N. Abdullah, The influence of alumina particle size on the properties and performance of alumina hollow fiber as support membrane for protein separation, Sep. Purif. Technol. 250 (2020), 117147, https://doi.org/10.1016/j.seppur.2020.117147.

[32] X.M. Tan, D. Rodrigue, A review on porous polymeric membrane preparation. Part II: production techniques with polyethylene, polydimethylsiloxane, polypropylene, polyimide, and polytetrafluoroethylene, Polymers 11 (2019) 1310, https://doi.org/10.3390/polym11081310.

[33] M. Niknam Shahrak, M. Ghahramaninezhad, M. Eydifarash, Zeolitic imidazolate framework-8 for efficient adsorption and removal of Cr(VI) ions from aqueous solution, Environ. Sci. Pollut. Res. 24 (2017) 9624–9634, https://doi.org/10.1007/s11356-017-8577-5.

[34] N.M. Mahpoz, N. Abdullah, M.Z.M. Pauzi, M.A. Rahman, K.H. Abas, A.A. Aziz, M. H.D. Othman, J. Jaafar, A.F. Ismail, Synthesis and performance evaluation of zeolitic imidazolate framework-8 membranes deposited onto alumina hollow fiber for desalination, Korean J. Chem. Eng. 36 (2019) 439–449, https://doi.org/10.1007/s11814-018-0214-6.

[35] N.A.H.M. Nordin, A.F. Ismail, N. Misdan, N.A.M. Nazri, Modified ZIF-8 mixed matrix membrane for CO_2/CH4 separation, AIP Conf. Proc. 1891 (2017), 020091, https://doi.org/10.1063/1.5005424.

[36] K. Kida, K. Fujita, T. Shimada, S. Tanaka, Y. Miyake, Layer-by-layer aqueous rapid synthesis of ZIF-8 films on a reactive surface, Dalton Trans. 42 (2013) 11128, https://doi.org/10.1039/c3dt51135a.

[37] P.H. Chang, Y.T. Lee, C.H. Peng, Synthesis and characterization of hybrid metal zeolitic imidazolate framework membrane for efficient H_2 /Co_2 gas separation, Materials 13 (2020) 1–15, https://doi.org/10.3390/ma13215009.

[38] E. Shamsaei, Z.X. Low, X. Lin, A. Mayahi, H. Liu, X. Zhang, J. Zhe Liu, H. Wang, Rapid synthesis of ultrathin, defect-free ZIF-8 membranes via chemical vapour modification of a polymeric support, Chem. Commun. 51 (2015) 11474–11477, https://doi.org/10.1039/c5cc03537f.

[39] J. Cravillon, C.A. Schröder, H. Bux, A. Rothkirch, J. Caro, M. Wiebcke, Formate modulated solvothermal synthesis of ZIF-8 investigated using time-resolved in situ X-ray diffraction and scanning electron microscopy, CrystEngComm 14 (2012) 492–498, https://doi.org/10.1039/C1CE06002C.

[40] O.M. Linder-Patton, T.J. De Prinse, S. Furukawa, S.G. Bell, K. Sumida, C.J. Doonan, C.J. Sumby, Influence of nanoscale structuralization on the catalytic performance of ZIF-8: a cautionary surface catalysis study, CrystEngComm 20 (2018) 4926–4934, https://doi.org/10.1039/c8ce00746b.

[41] K. Huang, Z. Dong, Q. Li, W. Jin, Growth of a ZIF-8 membrane on the inner-surface of a ceramic hollow fiber via cycling precursors, Chem. Commun. 49 (2013) 10326–10328, https://doi.org/10.1039/c3cc46244g.

[42] X. Wu, C. Liu, J. Caro, A. Huang, Facile synthesis of molecular sieve membranes following "like grows like" principle, J. Memb. Sci. 559 (2018) 1–7, https://doi.org/10.1016/j.memsci.2018.04.053.

[43] H. Zhang, J. Nai, L. Yu, X.W. (David) Lou, Metal-organic-framework-based materials as platforms for renewable energy and environmental applications, Joule 1 (2017) 77–107, https://doi.org/10.1016/j.joule.2017.08.008.

[44] Y. Li, A. Pang, C. Wang, M. Wei, Metal-organic frameworks: promising materials for improving the open circuit voltage of dye-sensitized solar cells, J. Mater. Chem. 21 (2011) 17259–17264, https://doi.org/10.1039/c1jm12754c.

[45] O.O. Ltaief, S. Siffert, S. Fourmentin, M. Benzina, Synthesis of Faujasite type zeolite from low grade Tunisian clay for the removal of heavy metals from aqueous waste by batch process: kinetic and equilibrium study, C. R. Chim. 18 (2015) 1123–1133, https://doi.org/10.1016/j.crci.2015.03.013.

[46] N. Bakhtiari, S. Azizian, Adsorption of copper ion from aqueous solution by nanoporous MOF-5: a kinetic and equilibrium study, J. Mol. Liq. 206 (2015) 114–118, https://doi.org/10.1016/j.molliq.2015.02.009.

[47] K.Y. Foo, B.H. Hameed, Insights into the modeling of adsorption isotherm systems, Chem. Eng. J. 156 (2010) 2–10, https://doi.org/10.1016/j.cej.2009.09.013.

[48] F. Haghseresht, G.Q. Lu, Adsorption characteristics of phenolic compounds onto coal-reject-derived adsorbents, Energy Fuels 12 (1998) 1100–1107, https://doi.org/10.1021/ef9801165.

[49] N. Muhamad, N. Abdullah, M.A. Rahman, K.H. Abas, A.A. Aziz, Removal of nickel from aqueous solution using supported zeolite-Y hollow fiber membranes, Environ. Sci. Pollut. Res. 25 (2018) 19054–19064.

[50] S. Ersali, V. Hadadi, O. Moradi, A. Fakhri, Pseudo-second-order kinetic equations for modeling adsorption systems for removal of ammonium ions using multi-walled carbon nanotube, Fuller. Nanotub. Carbon Nanostruct. (2013), https://doi.org/10.1080/1536383x.2013.787610, 150527104639002.

[51] Q. Wang, S. Zhang, X. Ji, F. Ran, High rejection performance ultrafiltration membrane with ultrathin dense layer fabricated by movement and dissolving of metal-organic frameworks, New J. Chem. (2020), https://doi.org/10.1039/D0NJ02700F.Volume.

[52] M.A. Tofighy, T. Mohammadi, Synthesis and characterization of ceramic/carbon nanotubes composite adsorptive membrane for copper ion removal from water, Korean J. Chem. Eng. 32 (2014) 292–298, https://doi.org/10.1007/s11814-014-0210-4.

[53] A. Ali, A. Ahmed, A. Gad, Chemical and microstructural analyses for heavy metals removal from water media by ceramic membrane filtration, Water Sci. Technol. 75 (2017) 439–450, https://doi.org/10.2166/wst.2016.537.

[54] K. Wang, Z. Tian, N. Yin, Significantly enhancing Cu(II) adsorption onto Zr-MOFs through novel cross-flow disturbance of ceramic membrane, Ind. Eng. Chem. Res. 57 (2018) 3773–3780, https://doi.org/10.1021/acs.iecr.7b04850.

[55] N. Ghaemi, A new approach to copper ion removal from water by polymeric nanocomposite membrane embedded with γ-alumina nanoparticles, Appl. Surf. Sci. 364 (2016) 221–228, https://doi.org/10.1016/j.apsusc.2015.12.109.

[56] S. Abd Hamid, M. Shahadat, B. Ballinger, S. Farhan Azha, S. Ismail, S. Wazed Ali, S. Ziauddin Ahammad, Role of clay-based membrane for removal of copper from aqueous solution, J. Saudi Chem. Soc. 24 (2020) 785–798, https://doi.org/10.1016/j.jscs.2020.08.007.